Research

New Phytologist

ENHANCED GRAVITROPISM 2 coordinates molecular adaptations to gravistimulation in the elongation zone of barley roots

Li Guo[1], Alina Klaus[1], Marcel Baer[1], Gwendolyn K. Kirschner[1], Silvio Salvi[2] and Frank Hochholdinger[1]

[1]Institute of Crop Science and Resource Conservation, Crop Functional Genomics, University of Bonn, 53113 Bonn, Germany; [2]Department of Agricultural and Food Sciences, University of Bologna, 40127 Bologna, Italy

Author for correspondence:
Frank Hochholdinger
Email: hochholdinger@uni-bonn.de

Received: *11 October 2022*
Accepted: *11 December 2022*

New Phytologist (2023) **237:** 2196–2209
doi: 10.1111/nph.18717

Key words: barley, bimolecular fluorescence complementation (BiFC), EGT2, gravitropism, RNA-seq, WGCNA, yeast-two-hybrid.

Summary

- Root gravitropism includes gravity perception in the root cap, signal transduction between root cap and elongation zone, and curvature response in the elongation zone. The barley (*Hordeum vulgare*) mutant *enhanced gravitropism 2* (*egt2*) displays a hypergravitropic root phenotype.
- We compared the transcriptomic reprogramming of the root cap, the meristem, and the elongation zone of wild-type (WT) and *egt2* seminal roots upon gravistimulation in a time-course experiment and identified direct interaction partners of EGT2 by yeast-two-hybrid screening and bimolecular fluorescence complementation validation.
- We demonstrated that the elongation zone is subjected to most transcriptomic changes after gravistimulation. Here, 33% of graviregulated genes are also transcriptionally controlled by *EGT2*, suggesting a central role of this gene in controlling the molecular networks associated with gravitropic bending. Gene co-expression analyses suggested a role of *EGT2* in cell wall and reactive oxygen species-related processes, in which direct interaction partners of EGT2 regulated by *EGT2* and gravity might be involved.
- Taken together, this study demonstrated the central role of *EGT2* and its interaction partners in the networks controlling root zone-specific transcriptomic reprogramming of barley roots upon gravistimulation. These findings can contribute to the development of novel root idiotypes leading to improved crop performance.

Introduction

The gravitropic response plays an essential role in controlling plant growth direction and architecture under changing environmental conditions (Nakamura *et al.*, 2019). Root gravitropism enables plants to adjust their root growth direction, allowing them to penetrate deeply into the soil, thereby anchoring plants in the soil and optimizing the uptake of water and nutrients (Zhang *et al.*, 2019). In flowering plants, root gravitropic response is a three-step process: gravity perception, signal transduction, and curvature response (Singh *et al.*, 2017; Su *et al.*, 2017; Nakamura *et al.*, 2019; Jiao *et al.*, 2021).

The most prominent explanation of how roots sense gravity is the starch-statolith hypothesis: Upon root reorientation, the gravity signal is sensed by starch-filled amyloplasts sedimented to the new bottom-site of the columella cells in the root cap (Singh *et al.*, 2017; Su *et al.*, 2017). This results in the relocalization of auxin toward the bottom side of columella cells by downward auxin transport and a lateral auxin gradient across the root cap. Auxin is then transported to the lateral root cap and epidermal cells in a shootward direction toward the elongation zone, resulting in asymmetrical auxin distribution across the distal elongation zone with higher auxin levels on the lower flank and lower auxin content on the upper flank. In the epidermal cells on the lower flank of the elongation zone, elevated auxin levels increase the apoplastic pH and inhibit cell elongation. By contrast, on the upper side of the elongation zone, decreased auxin levels lead to a decrease in the pH of the apoplast, which increases cell elongation. The asymmetrical elongation of cells on the two sides of the gravistimulated root eventually leads to the gravitropic root bending in the direction of gravity (Su *et al.*, 2020). Nevertheless, cells within the root distal elongation zone have also been shown to play a role in gravity perception with an alternative mechanism (Wolverton *et al.*, 2002; Mancuso *et al.*, 2006; Su *et al.*, 2020).

In a previous study, we identified the barley mutant *egt2* (*enhanced root gravitropism 2*) that displays a narrower root system

than wild-type (WT) plants, with root angles at least 50% smaller than WT. Phytohormone treatment showed that *egt2* responds to auxin similarly as the WT, suggesting that the auxin response is unaffected in *egt2*. Moreover, we did not observe any significant differences between the structure and size of the meristem, the root cap, amyloplast content, and the amyloplast sedimentation velocities between *egt2* and WT. This suggests that *EGT2* is likely involved in root gravitropism after gravity perception. The *EGT2* gene encodes a STERILE ALPHA MOTIF (SAM) domain–containing protein (Kirschner *et al.*, 2021). STERILE ALPHA MOTIF domains are present in thousands of proteins in prokaryotes and diverse eukaryotes (Kim & Bowie, 2003; Qiao & Bowie, 2005; Denay *et al.*, 2017). The SAM domain was first considered as an evolutionarily conserved protein binding domain (Schultz *et al.*, 1997). Subsequently, a large diversity of SAM functions has been observed, including the binding of proteins, lipids, and RNAs (Denay *et al.*, 2017; Ray *et al.*, 2020). The best-characterized plant SAM domain-containing protein is LEAFY that functions as a master regulator of flower development in angiosperms (Eriksson *et al.*, 2006; Siriwardana & Lamb, 2012; Yamaguchi, 2021). The SAM domain at the N-terminus of LEAFY mediates oligomerization of LEAFY, which allows the LEAFY dimers to bind to DNA regions without LEAFY-binding sites or closed chromatin regions (Sayou *et al.*, 2016). AtSAM5, a homolog of EGT2 in Arabidopsis, has been shown to interact with the Ca^{2+}-dependent protein kinase CPK13 (Jones *et al.*, 2014), which is involved in the response to light by controlling the stomatal aperture (Ronzier *et al.*, 2014). Moreover, narrower lateral root angles were observed in mutants of *AtSAM5*, suggesting a role of *AtSAM5* in regulating lateral root angle in Arabidopsis (Johnson *et al.*, 2022). Another homolog of EGT2 is WEEP in peach trees (Hollender *et al.*, 2018). A 5′ deletion of the *WEEP* gene caused downward and wandering growth of the mutant shoots that did not bend upward after 90° reorientation. This suggests a role of WEEP in shoot gravitropism, which shows similarities to the function of EGT2 in roots (Hollender *et al.*, 2018). In barley, 17 SAM domain-containing proteins were annotated, and none of them has been functionally characterized thus far except for *EGT2* (Kirschner *et al.*, 2021).

In this study, the transcriptomes of the root cap, the meristem, and the elongation zone of gravistimulated WT and mutant *egt2* roots were studied by RNA sequencing (RNA-seq) in a time-course experiment. These experiments revealed that EGT2 is a central regulator of the gravitropism-regulated gene expression networks in barley seminal roots. Functional enrichment analyses of differentially expressed genes (DEGs) and weighted gene co-expression network analyses suggested the involvement of plant cell wall organization and reactive oxygen species (ROS) in *EGT2*-regulated root gravitropism. By a combination of yeast-two-hybrid experiments and bimolecular fluorescence complementation (BiFC), we demonstrated that a subset of the genes transcriptionally regulated by gravistimulation and by *EGT2* encoded proteins that directly interact with EGT2. The results of this study highlight the transcriptomic reprogramming of the gravitropic response of barley roots and provide new insights into the molecular function of *EGT2*.

Materials and Methods

Plant materials and growth condition

Wild-type barley plants (*Hordeum vulgare* L. cv Morex) and the *egt2* mutant (Kirschner *et al.*, 2021) were used for this study. Before germination, the seeds were washed in sodium hypochlorite (1.2% active chlorine) for 5 min and rinsed with distilled water. Then, seeds were incubated in dark at 30°C O/N, and only germinating seeds were used for further experiments. Plants used for RNA-seq were grown in growth chambers (Conviron, Winnipeg, MB, Canada) at 18°C at night (8 h) and 22°C at day (16 h).

Determination of root zones

To measure the length of the meristem, 3-d-old WT and *egt2* plants were rotated by 90° for 6 or 10 h. Root tip segments of 5 mm length of the most vertical roots before rotation were taken before and after rotation. Root tips were then embedded in 10% (w/v) agarose, and 40 µm sections were prepared with a vibratome. Images of root sections taken with a Zeiss PALM MicroBeam microscope (Zeiss) were analyzed by ImageJ. The zone between the first cell in the first cortical layer that doubled in size and the first cell that increased noticeably in length was considered as the transition zone. The length from root cap junction to the middle of transition zone was measured as the length of the meristem (Verbelen *et al.*, 2006; Baluška *et al.*, 2010). Eleven to nineteen roots were analyzed per genotype by time point combination (Supporting Information Fig. S1).

Sample collection and RNA isolation

For RNA sequencing, 3-d-old plants were rotated by 90° for 3, 6, and 12 h. The root cap, the meristem (1 mm; Fig. S1), and 1 mm of the distal elongation zone (Fig. 1a) of the most vertically grown seminal roots before rotation were separated by a razor blade under a binocular before (time point 0 h) and after rotation. Three roots were collected per seedling, and root zones from eight plants were pooled per biological replicate. Three biological replicates were used for each genotype by time point combination. After dissection, samples were immediately frozen in liquid nitrogen for RNA isolation. RNA extraction was performed with the RNeasy Plant Mini Kit (Qiagen) according to the manufacturer's protocol. RNA quality was assessed with an Agilent 2100 Bioanalyzer using the Agilent RNA 6000 Nano kit (Agilent, Santa Clara, CA, USA). The RNA integrity number was between 8.3 and 10 for all samples.

RNA-seq and data analyzing

Messenger RNA (mRNA) purified from total RNA using poly-T oligo-attached magnetic beads was used to prepare cDNA libraries for Illumina sequencing (Illumina, San Diego, CA, USA). Fragmented mRNA and random hexamer primers were used for reverse transcription. The cDNA library was prepared by ligating the cDNA product to adapter, followed by amplification

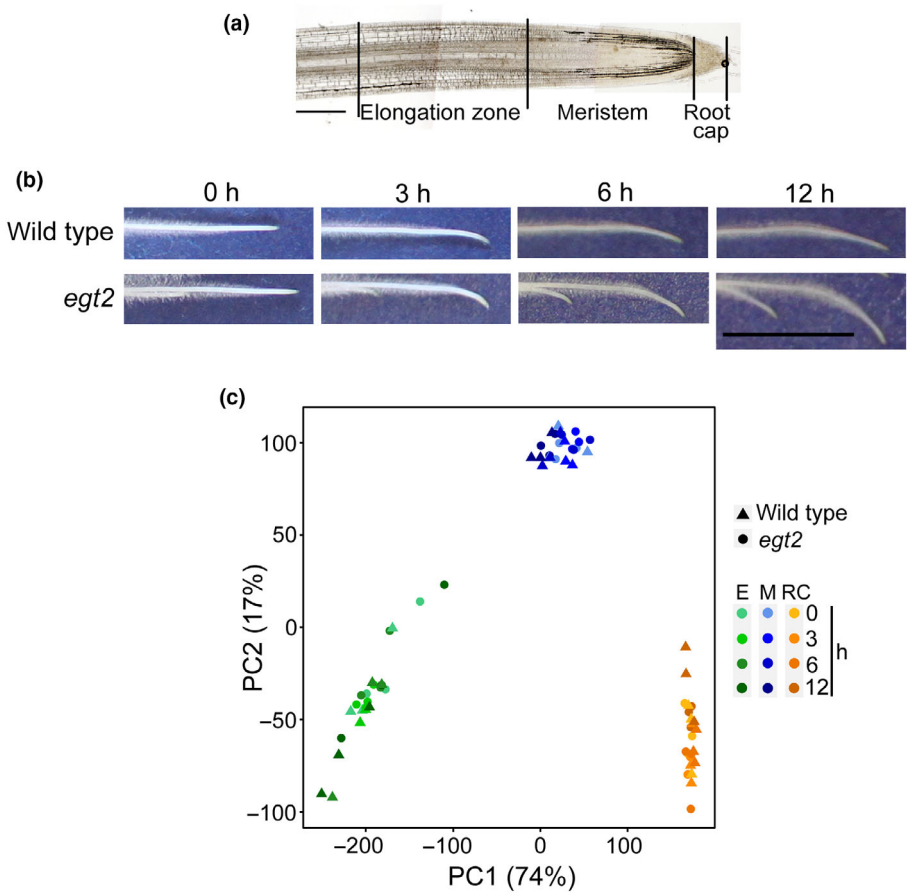

Fig. 1 Seminal roots upon rotation and RNA sequencing sample relationship of root zones. (a) Representative section for meristem length measurement, illustrating the elongation zone, the meristem, and the root cap harvested for RNA-seq. Bar, 300 μm. (b) Phenotype of wild-type and *enhanced gravitropism 2* mutant roots before (0 h) and after 3, 6, and 12 h of rotation. Bar, 1 cm. (c) Principal component analysis plot for the transcriptomes of the 72 RNA-seq samples of the two genotypes, three root zones, and four time points.

and purification (Novogene, Cambridge, UK). Cluster preparation and single read sequencing were performed according to the manufacturer's instructions (Illumina). Sequencing was performed in a NovaSeq 6000, S4 FlowCell using the paired-end 150 bp sequencing strategy. Raw RNA-seq reads were processed with CLC GENOMICS WORKBENCH (v.20.0.1) as previously described with some minor modifications (Osthoff *et al.*, 2019). Reads with a length < 40 bp were discarded, and the remaining reads were mapped to the barley reference genome (Hv_Morex.pgsb.Jul2020) with a similarity of 0.9 and a length fraction of 0.8. Reads mapped to more than one position were regarded as duplicate mapped reads and removed from further analyses (Mascher *et al.*, 2021).

Data generated by CLC GENOMICS WORKBENCH were analyzed using R. To remove lowly expressed genes, the cpm() function from the EDGER library was used to normalize the different sequencing depths for each sample (Robinson *et al.*, 2010). A CPM threshold of 1.2 was used and only genes that have at least three TRUES in each row of threshold were kept for further steps. A principal component analysis (PCA) was computed by R the functions prcomp() and visualized by the autoplot() function in the GGPLOT2 package. The contrasts.fit function of the R package LIMMA was used to calculate $\log_2$ fold change ($\log_2$FC) values between different root zones and time point combinations in the WT time-course experiment and in comparisons between the *egt2* mutant and WT (Ritchie *et al.*, 2015). The false discovery rate (FDR) was adjusted to < 5% to correct *P*-values of contrasts for multiple testing (Benjamini & Hochberg, 1995). Venn diagrams were produced by the VENNDIAGRAM package (Chen & Boutros, 2011). A hierarchical clustering analysis was conducted by the CLUSTER package with dynamic tree cutting (Maechler *et al.*, 2022). The upset() function in the UPSETR library was used for comparison between multiple gene sets (Conway *et al.*, 2017). Gene Ontology (GO) analyses were performed by the R function TOPGO (Alexa & Rahnenführer, 2022). Redundant GO terms were filtered by REVIGO with a similarity ≤ 0.5 (Supek *et al.*, 2011).

Weighted gene correlation network analysis

The R package weighted gene correlation network analysis (WGCNA) was used for gene co-expression analyses (Langfelder & Horvath, 2008). After filtering out lowly expressed genes with < 50 total reads in the 24 samples of each root zone, the read data generated by CLC GENOMICS WORKBENCH were used as input. Samples were clustered using the hclust function. The outlier samples were determined by setting the cutheight to 50 for the root cap, 40 for the meristem, and 75 for the elongation zone. After removing outliers, the co-expression modules of each root zone dataset were generated by the one-step network construction function blockwiseModules with a soft threshold of 4 for the root cap and elongation zone and 6 for the meristem, and setting

TOMtype to 'signed'. To avoid small clusters, modules with < 30 genes were merged with their closest larger module using the cutreeDynamic function. The eigengene calculation of each module was performed using the moduleEigengenes function followed by the calculation of the module dissimilarity of eigengenes. Modules whose eigengenes were correlated > 0.8 were merged via the mergeCutHeight function with a cutHeight of 0.20. A unique color was then assigned to each merged module via the plotDendroAndColors function. The edge weight determined by the topology overlap measure (TOM) reflected the connectivity between two genes. The weight values across all edges of each gene in each module were calculated and exported for gene network visualization, which was achieved by CYTOSCAPE (v.3.9.1). To determine the hub genes of each module, we sorted the weight values of each edge from the highest to the smallest, and nodes with the top 1%, 0.1%, or 0.01% of weight were considered as hub genes based on the size of the module. Gene networks were analyzed with the 'Analyze Network' tool in CYTOSCAPE and the 'degree' values were considered to reduce the numbers of hub genes.

We calculated relationships between module eigengenes and traits using Pearson's correlation coefficients in R. Significant *P*-values of each module and trait correlation were calculated using the corPvalueStudent function. Modules with *P*-values ≤ 0.05 were considered as significantly correlated modules.

Yeast-two-hybrid library construction

Total RNA extracted from the whole root system of ten 5-d-old seedlings was used to generate the cDNA library, which was conducted with the 'Make Your Own 'Mate & Plate™' Library System' according to the manufacturer's instructions with minor modifications (Clontech, Saint Germain en Laye, France). Oligo-dT primers provided in the kit were used for first-strand cDNA synthesis with 2 μg total RNA as input. Amplification of cDNA was performed by using long-distance PCR with 25 cycles to generate 6–7 μg of ds cDNA. After purifying with CHROMA SPIN + TE-400 columns, ds cDNA library was transformed into yeast (*Saccharomyces cerevisiae*) strain Y187.

Generation of competent yeast cells and library transformation were conducted using the LiAc/SS-DNA/PEG procedure (Gietz *et al.*, 1995). Transformed cell plating and library cell harvesting were conducted according to the manufacturer's instructions.

Toxicity and autoactivation testing

To test the toxicity and autoactivation of EGT2, the full-length coding sequence of EGT2 was amplified using the primers specified in Table S1 and then inserted into the vector pGBKT7 using *Eco*RI and *Bam*HI restriction endonucleases. Detection of EGT2 toxicity on yeast growth was performed according to Matchmaker® Gold Yeast Two-Hybrid System User Manual (TaKaRa, Saint Germain en Laye, France). Yeast cells expressing pGBKT7-EGT2 displayed a similar growth rate to yeast cells transformed with an empty pGBKT7 vector, indicating that EGT2 is not toxic (Fig. S2a). To test the autoactivation of EGT2, pGBKT7-EGT2 plasmid was co-transformed into Y2HGold yeast cells with pGADT7. pGBKT7-53 and pGBKT7-lam plasmids were transformed together with pGADT7-T as positive and negative controls, respectively. The transformed cells were grown on SD/−Trp/−Leu medium at 30°C for 4 d. Three clones of each combination were diluted in ddH_2O, and 1 μl of these diluted cells was dotted on SD/−Trp/−Leu/−His/−Ade medium and grown at 30°C for 4 d. Yeast cells transformed with pGBKT7-EGT2 plasmid cannot survive on SD−Trp/−Leu/−Ade/−His medium, suggesting that EGT2 does not display autoactivation (Fig. S2b). Therefore, pGBKT7-EGT2 was used as bait for yeast-two-hybrid screening.

Yeast-two-hybrid library screening

Yeast-two-hybrid library screening was performed according to the Matchmaker Gold Yeast Two-Hybrid System User Manual (Clontech).

Yeast colony PCR was performed with pGADT7 primers to eliminate duplicated positive colonies containing the same prey plasmid. Among the PCR products from all positive colonies, only DNA bands with different sizes were recovered and sequenced to identify the genes inserted. Subsequently, prey plasmids from library were rescued from yeast clones with 'Easy Yeast Plasmid Isolation Kit' (Clontech) and sequenced. By doing so, all prey plasmids contained in one positive colony were identified and further tested. These prey plasmids were further used in one-on-one yeast-two-hybrid assays to confirm the results of yeast-two-hybrid screening.

Subcellular localization

The vectors constructed using the 2in1 cloning system were used for the subcellular localization analyses (Grefen & Blatt, 2012). The full-length coding sequence of *EGT2* (*HORVU.MOREX.r3.5HG0447830.1*), *OMT* (*HORVU.MOREX.r3.3HG0330120.1*), *PBP* (*HORVU.MOREX.r3.7HG0709860.1*), *GXM* (*HORVU.MOREX.r3.7HG0749870.1*), *HMT* (*HORVU.MOREX.r3.2HG0126380.1*), and *HORVU.MOREX.r3.1HG0000050.1* was amplified using Phusion™ High-Fidelity DNA Polymerase (Thermo Fisher Scientific, Waltham, MA, USA) with primers specified in Table S1.

The insertion of the *EGT2* amplicons into pDONR221 P1-P4 entry vector carrying the attP1 and attP4 recombination sites was accomplished by BP reactions using the BP Clonase™ II enzyme mix (Thermo Fisher Scientific). The same enzyme was used for insertion of interaction candidates into pDONR221 P2R-P3 carrying the attP2 and attP3 recombination sites. Subsequently, entry clones were integrated with the corresponding destination vectors pFRETvr-2in1-NN or pFRETvr-2in1-NC. The reaction was catalyzed by LR Clonase™ II Mix (Thermo Fisher Scientific). Finally, we generated expression constructs containing the *EGT2* coding sequence either N- or C-terminally fused to tagRFP (EGT2-tagRFP and tagRFP-EGT2) and the coding sequence of interaction partners N-terminally fused to mVenus. All constructs were verified and transformed into Agrobacterium (*Agrobacterium tumefaciens*) strain AGI1.

Positive Agrobacterium clones were cultured in lysogeny broth medium with respective antibiotics until OD_{600} reach 0.8. Then, cells were precipitated and dissolved in 10 mM $MgCl_2$, 10 mM MES (2-morpholinoethanesulfonic acid), and 100 µM AS (Acetosyringone), and infiltrated into tobacco (*Nicotiana benthamiana*) leaves using a syringe. Transgene expression was analyzed using a Zeiss LSM 780 confocal microscopy system 3 d after infiltration. The fluorescence of tagRFP was excited at 543 nm using a helium neon laser with a laser power of 30%, and detected through the meta-channel at 579–633 nm (ChS1). mVenus and chloroplast autofluorescence were excited at 488 nm by the argon laser with a 10% laser power, emission of mVenus was detected at 517–553 nm. The emission of chloroplast autofluorescence was detected at 686–711 nm via the meta-channel (ChS2).

Bimolecular fluorescence complementation

The same entry vectors as used for the subcellular localization experiments were integrated with the corresponding destination vectors pBiFCt-2in1-NN or pBiFCt-2in1-NC for BiFC. Both destination vectors contained *tagRFP*, which was driven by the CaMV 35S promoter and used as a positive control for successful infiltration of tobacco cells. Finally, we generate expression constructs containing the *EGT2* coding sequence without stop codon (−TGA) N-terminally fused to the C-terminal part of YFP (EGT2 (−TGA)-cYFP) or the *EGT2* coding sequence with stop codon (+TGA) C-terminally fused to the C-terminal part of YFP (cYFP-EGT2 (+TAG)) and the coding sequence of the interaction partners C-terminally fused to the N-terminal part of YFP (nYFP-interaction partner (+TAG)). Constructs containing only the *EGT2* coding sequence either N- or C-terminally fused to cYFP were used to detect the autofluorescence of EGT2. Constructs containing the coding sequence of interaction partners C-terminally fused to nYFP and the coding sequence of *EGT2* with stop codon (+TAG) N-terminally fused to cYFP were used to detect the autofluorescence of interaction partners because cYFP will not be translated in this case. All constructs were verified and transformed into Agrobacterium strain AGI1. Tobacco infiltration and transgene expression analysis were conducted as described above. Excitation and detection of RFP, YFP (similar to mVenus), and chloroplast autofluorescence were performed as described above.

Results

Transcriptomic dynamics of three root zones of WT and *egt2* seminal roots upon gravistimulation

We investigated the transcriptomic dynamics in the root cap, the meristem, and the elongation zone (Fig. 1a) in seminal roots of WT seedlings and the hypergravitropic mutant *egt2* at 0, 3, 6, and 12 h after rotation by 90° (Fig. 1b) by RNA-seq (see the Materials and Methods section). Determination of the size of the different root zones is described in Fig. S1 and the material and methods section. We explored the transcriptomic relationship between genotypes, root zones, and duration of gravistimulation by a PCA (Fig. 1c). In the PCA plot, two components (PC1 and PC2) accounted for 91% of the total variance. The first component PC1 explained 74% of the overall variance and distinctly separated the samples of each root zone, indicating larger transcriptomic differences between root zones than between genotypes and time points (Fig. 1c).

Determination of genes responding to gravistimulation in seminal root zones

To identify genes responding to gravistimulation in barley roots, three pairwise comparisons were computed between control (0 h) and gravistimulated (3, 6, and 12 h) root samples for each of the three zones of WT roots. We determined DEGs using a FDR < 5% (Fig. 2a). In all three zones, longer gravitropic stimulation resulted in more DEGs (Fig. 2a; Table S2). The lowest number of identified genes at each time point was observed in the meristem (Fig. 2a). Only five genes were differentially regulated in the meristem (M) 12 h after rotation (Fig. 2a). Of 462 distinct DEGs in the root cap (RC), none was differentially expressed at all three time points after gravistimulation (Fig. 2b). Similarly, of 3173 distinct DEGs in the elongation zone (E), only the seven genes that were already induced 3 h after treatment were consistently regulated at all three time points (Fig. 2c). This suggests for both root zones, that most gravistimulated genes are specifically stimulated after a certain period of gravitropic bending (Fig. 2b,c). By investigating the expression dynamics of genes – whose homologs have been reported to play a role in regulating root gravitropism, we found that *HORVU.MOREX.r3.2HG0125600.1*, a homolog of *AtLZY2* and *AtLZY3* (Taniguchi *et al.*, 2017), and *HORVU.MOREX.r3.5HG0509060.1*, a homolog of *ZmCIPK15* (Schneider *et al.*, 2022), were significantly downregulated in the root cap after 12 h of gravistimulation (Table S2).

Expression dynamics of DEGs regulated by gravistimulation in seminal roots

To group genes with similar expression patterns over 12 h of rotation, we performed hierarchical clustering of all DEGs in the root cap and the elongation zone of WT roots. Hierarchical clustering classified 462 DEGs in the root cap into three clusters (Fig. S3a,b; Table S3) and 3173 DEGs in the elongation zone into nine clusters (Fig. S3c,d; Table S4) according to different patterns of up- and downregulation in the course of gravistimulation.

Gene Ontology term analyses assigned a variety of biological functions to the genes enriched in each cluster (Table S5). A number of enriched biological process terms related to cell wall were shared between different clusters in the elongation zone. For instance, the term 'plant-type cell wall organization' (GO:0009664); 'xyloglucan metabolic process' (GO:0010411); 'fucose metabolic process' (GO:0006004); and 'cellulose biosynthetic process' (GO:0030244) were shared between several clusters (Table S5b). In addition, the terms 'response to oxidative stress' (GO:0006979), 'hydrogen peroxide catabolic process'

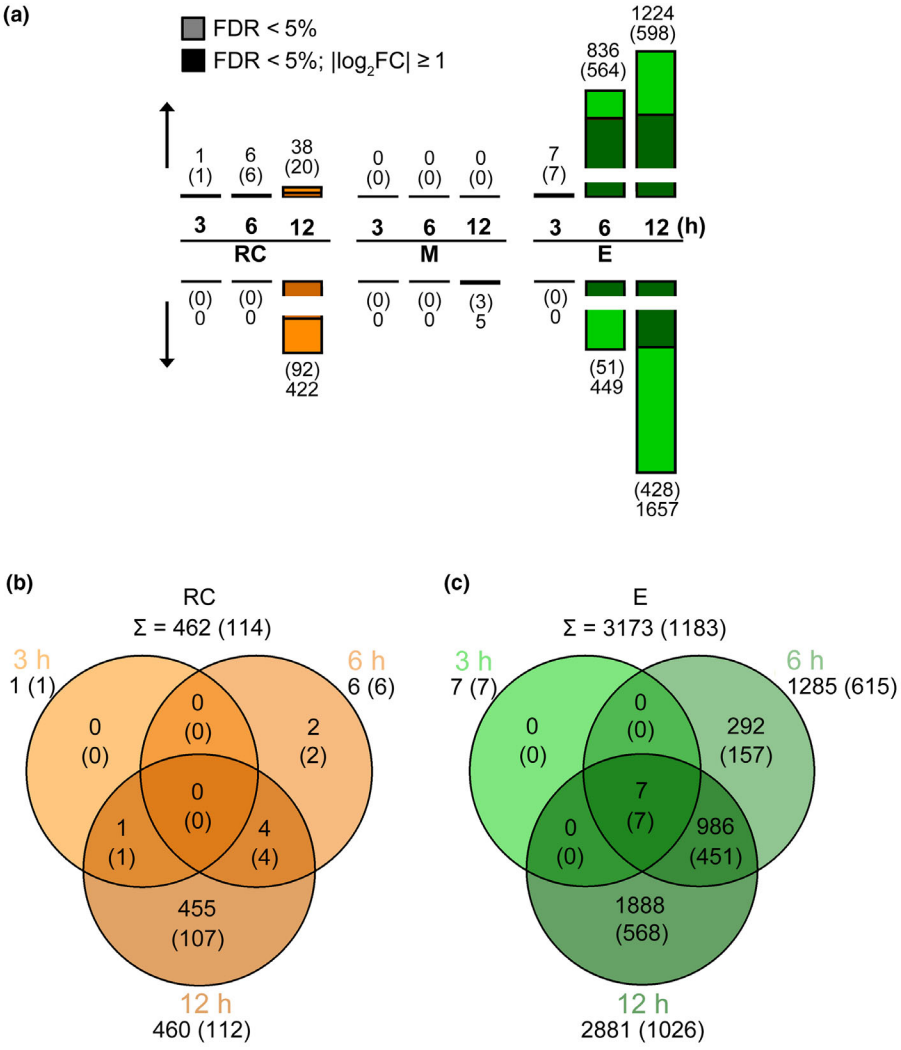

Fig. 2 Differential gene expression in gravistimulated wild-type (WT) roots. (a) Numbers of up- (↑) and downregulated (↓) genes determined by three pairwise comparisons between the root zones of WT vertically grown roots and the corresponding zone of WT gravistimulated roots. RC, root cap; M, meristem; E, elongation zone (light color and numbers without brackets, false discovery rate (FDR) < 5%; dark color and numbers in brackets, FDR < 5%, $\log_2$ fold change ($|\log_2 FC| \geq 1$). (b, c) Venn diagram of differentially regulated genes by gravistimulation in WT root cap (b) and elongation zone (c) (numbers without brackets, FDR < 5%; numbers in brackets, FDR < 5%, $|\log_2 FC| \geq 1$).

(GO:0042744), and 'protein phosphorylation' (GO:0006468) were significantly enriched in multiple clusters (Table S5b).

Determination of DEGs between gravistimulated roots of *egt2* and WT

Differential genes expression between *egt2* and WT was determined for each root zone by time point combination by computing 12 pairwise contrasts (Fig. 3a; Table S6). The root cap displayed 126 (Fig. 3b), the meristem 62 (Fig. 3c), and the elongation zone 2982 unique DEGs (Fig. 3d). In comparison with the WT, *EGT2* was downregulated in all three root zones of the *egt2* mutant at all four time points (Table S6).

Gene Ontology analyses revealed that 31 biological process terms were assigned to DEGs in the root cap (Table S7a). Among them, 'cytoplasmic microtubule organization' (GO:0031122), 'trichome branching' (GO:0010091), and 'plant-type cell wall biogenesis' (GO:0009832) were conserved among upregulated genes at all four time points (Table S7a). In the meristem, 17 GO terms were enriched (Table S7b). As in the root cap, the GO terms 'cytoplasmic microtubule organization' (GO:0031122), 'trichome branching' (GO:0010091), and 'plant-type cell wall biogenesis' (GO:0009832) were conserved among upregulated genes at all four time points in the meristem. In addition, 'cell growth' (GO:0016049) was conserved among upregulated genes while 'one-carbon metabolic process' (GO:0006730) was conserved among downregulated genes at all four time points (Table S7b). Finally, we identified 113 significantly enriched GO terms in the DEGs of the elongation zone (Table S7c). Among those, five GO terms were conserved among upregulated genes at 0, 3, and 6 h, while six GO terms were enriched among downregulated genes at 0 and 3 h, and among upregulated genes at 12 h (Table S7c).

Identification of genes regulated by gravity and by *EGT2*

To screen for genes, which are regulated by gravistimulation and *EGT2*, we compared DEGs responding to gravitropic stimulus with DEGs determined in *egt2* vs WT comparisons. We observed 13 intersecting genes in the root cap (Fig. 4a) and 1038 genes in the elongation zone (Fig. 4b). These genes are listed in Table S8. Among these genes, 12 of 13 in the root cap and 1027 of 1038 in

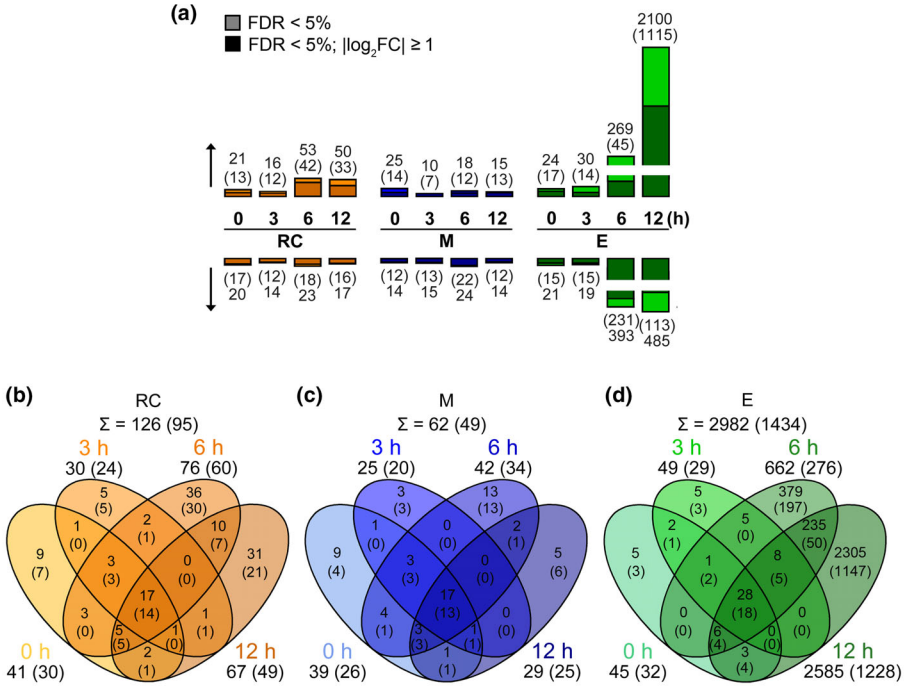

Fig. 3 Differential gene expression between *egt2* mutant and wild-type (WT). (a) Numbers of up- (↑) and downregulated (↓) genes identified by pairwise comparisons between the *egt2* mutant and WT for each of the three root zones: root cap (RC), meristem (M), and elongation zone (E) at each of the four time points: 0, 3, 6, and 12 h (light color and numbers without brackets, false discovery rate (FDR) < 5%; dark color and numbers in brackets, FDR < 5%, $\log_2$ fold change ($|\log_2 FC| \geq 1$). (b–d) Overlap of differentially expressed genes between the four time points in the root cap (b), the meristem (c), and the elongation zone (d) of *egt2* vs WT (numbers without brackets, FDR < 5%; numbers in brackets, FDR < 5%, $|\log_2 FC| \geq 1$).

the elongation zone showed opposite regulatory directions in WT time-course experiments and in *egt2* vs WT comparisons. No *EGT2*-regulated gene responding to gravistimulation was identified in the meristem. Of the gravity-regulated genes, 3% in the root cap and 33% in the elongation zone were also regulated by *EGT2*.

We conducted GO analyses for these intersected genes to reveal the biological processes in which *EGT2* might be involved to regulate root gravitropism. Three protein transmembrane transport-related and two mitochondrion-related GO terms were significantly enriched in intersected DEGs in the root cap (Fig. S4a). Of the 26 GO terms significantly enriched among the overlapping genes in the elongation zone, seven terms were associated with plant cell wall organization, four terms were related to protein processing, two terms were ROS-related, and two terms were associated with carbohydrate metabolic processes (Fig. S4b).

Identification of co-expression networks and their association with the traits genotype and time of gravistimulation

To reveal additional genes that are significantly associated with *EGT2* and gravistimulation in the root cap, meristem, and elongation zone of barley seminal roots, we performed a weighted gene co-expression network analysis (WGCNA). We constructed a co-expression network for the RNA sequencing data separately for each root zone to eliminate the effect of the large expression differences between the distinct root zones on the following analyses. This analysis identified 13 co-expression modules in the root cap, 21 in the meristem, and nine in the elongation zone (Fig. S5a–c). These modules were then correlated with the two genotypes (WT and *egt2*) and the time of gravistimulation (0, 3, 6, and 12 h). This resulted in nine modules that are strongly correlated (*) with at least one trait in the root cap (Fig. 5a), 14 in the meristem (Fig. 5b), and six in the elongation zone (Fig. 5c) with the module size ranging from 38 to 11 791 genes.

We determined two modules that were significantly correlated with genotype, and modules that displayed contrasting correlation values between WT and *egt2* at some time points in all three root zones (Fig. 5a–c). We performed GO analyses to identify overrepresented biological processes among genes in the three most strongly correlated modules in each root zone. The five most significantly enriched biological process terms in each module are shown in Fig. S5(d). Noticeably, 'plant-type cell wall organization' (GO:0009664), 'response to oxidative stress' (GO: 0006979), and 'hydrogen peroxide catabolic processes' (GO:0042744) were consistently identified in modules that significantly correlated with genotype in all three root zones (Fig. S5d). We compared genes associated with plant cell wall and ROS-related processes between the three root zones (Fig. 5d–f). Results showed that *HORVU.MOREX.r3.6HG0611780* and six genes encoding peroxidases were included in significantly correlated modules in all three root zones (Fig. 5d–f). All six genes encoding peroxidases were regulated by gravistimulation in the elongation zone, two of which were regulated by *EGT2* (Fig. 5g).

The module hub genes are defined as genes that are high connected with other genes in the module and have been shown to be closely correlated with biological processes. We determined hub genes in the three most strongly correlated modules in each root zone and surveyed their expression levels in WT gravistimulation time-course experiments and in *egt2* vs WT comparisons (Fig. S5e–g). Among them, *EGT2* was considered as a hub gene

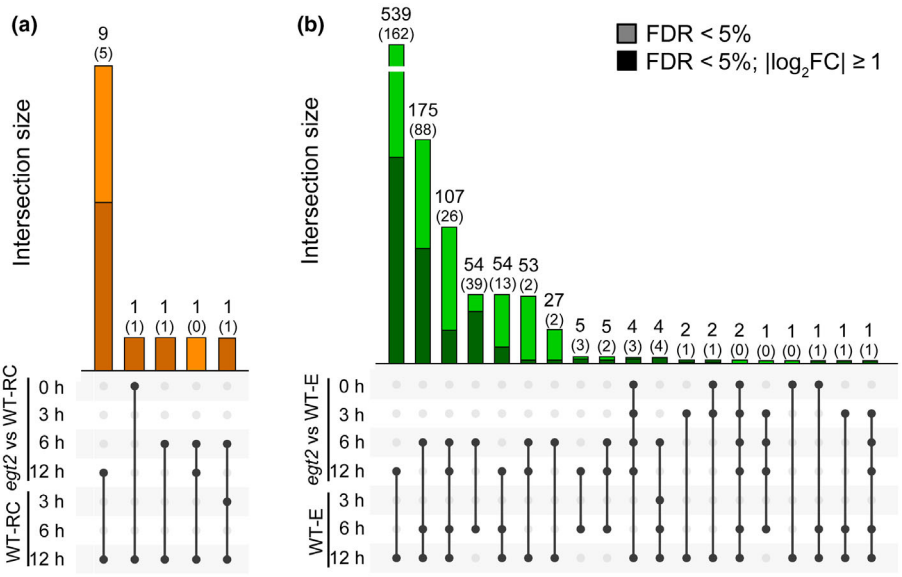

Fig. 4 Intersections between differentially expressed genes (DEGs) in the wild-type (WT) time-course experiment and in *egt2* vs WT comparisons. (a, b) Overlap of DEGs in the root cap (a) and elongation zone (b) of gravistimulated roots of the WT time-course and *egt2* vs WT comparisons (numbers without brackets, false discovery rate (FDR) < 5%; numbers in brackets, FDR < 5%, $\log_2$ fold change ($|\log_2 FC| \geq 1$).

in the midnightblue module in the meristem (Fig. S5f). All seven hub genes identified in this module displayed an *EGT2*-regulated while gravity-independent expression pattern (Fig. S5f). Hub genes identified in selected modules in the elongation zone were regulated by either gravity or *EGT2* in the elongation zone, seven of them were regulated by gravity and *EGT2* (Fig. S5g).

Identification of the interaction partners of EGT2 by a yeast-two-hybrid screening

To determine whether some of these DEGs are encoding for interaction partners of EGT2, we performed a yeast-two-hybrid screening. Two yeast-two-hybrid screens yielded 79 putative interaction partners of EGT2 that were confirmed by Sanger sequencing (Fig. S2c; Table S9). To validate this result in yeast cells, we tested the interaction between EGT2 and 23 putative interaction candidates by a one-on-one yeast-two-hybrid assay. The 23 interaction candidates included 21 candidates that were captured more than twice and two candidates encoded by DEGs in *egt2* vs WT comparisons (Fig. S2d; Table S9). Yeast cells co-transformed with EGT2 and the 23 selected interaction candidates survived and turned blue on high stringency selective medium (SD−Leu/−Trp/−His/−Ade + AbA + X-a-Gal), while yeast cells transformed with the empty control vector together with these 23 candidates could not grow on this medium (Fig. S2d). This suggests that all 23 selected interactions were positive in yeast cells (Fig. S2d), which confirmed the validity of the yeast-two-hybrid results.

Of all genes encoding putative interaction candidates, three genes were differentially expressed in the root cap and 24 in the elongation zone of gravity-stimulated WT roots. Moreover, 16 genes were differentially expressed in the elongation zone of the *egt2* mutant compared with WT (Fig. S2e; Table S9). Among those, genes encoding eight interaction partners were regulated by gravistimulation and *EGT2* (Table S9). Comparisons between the expected (= number of interaction candidates: number of annotated gene models × number of DEGs) and the observed number of interaction partners in each data set showed that more interaction partners were observed in the elongation zone of WT roots than expected after 6 and 12 h of rotation (Fig. S2e).

Validation of selected EGT2 interaction partners by BiFC

Five of eight interaction partners encoded by gravity and *EGT2*-regulated genes were independently surveyed via BiFC (Table S9). We first investigated the subcellular localization of EGT2 and the five interaction partners by fusing tagRFP to the N-terminus of EGT2 (Fig. 6a: tagRFP-EGT2) and fusing mVenus to the N-terminus of the interaction partners (Fig. 6a: mVenus-interaction partner). This experiment demonstrated that EGT2 and the four interaction candidates, HORVU.MOREX.r3.3HG0330120.1 (OMT), HORVU.MOREX.r3.7HG0709860.1 (PBP), HORVU.MOREX.r3.7HG0749870.1 (GXM), and HORVU.MOREX.r3.2HG0126380.1 (HMT) localized to the cytoplasm and the nucleus (Fig. 6a: results for mVenus-OMT, mVenus-GXM and mVenus-HMT). However, we were not able to detect the subcellular localization signal of HORVU.MOREX.r3.1HG0000050.1. For the BiFC assay, the four interaction candidates that also co-localized with EGT2 were C-terminally fused to the N-terminal fragment of YFP (Fig. 6b: nYFP-OMT, nYFP-GXM, nYFP-HMT), while EGT2 was either N-terminally (Fig. 6b: EGT2 (−TGA)-cYFP) or C-terminally (Fig. 6b: cYFP-EGT2 (+TGA)) fused to cYFP. We detected yellow fluorescence signals emitted by the interactions in tobacco epidermal cells infiltrated with constructs containing nYFP-OMT or nYFP-GXM and cYFP-EGT2 (+TGA) and the construct containing nYFP-HMT and EGT2 (−TGA)-cYFP (Fig. 6b). We did not detect a yellow fluorescence signal in tobacco epidermal cells infiltrated with constructs containing the coding sequence of EGT2 fused to cYFP (Fig. S6: cYFP-EGT2 (+TGA), EGT2 (−TGA)-cYFP) and the coding sequence of nYFP (Fig. S6). Nor did we detect a YFP signal in tobacco

New Phytologist

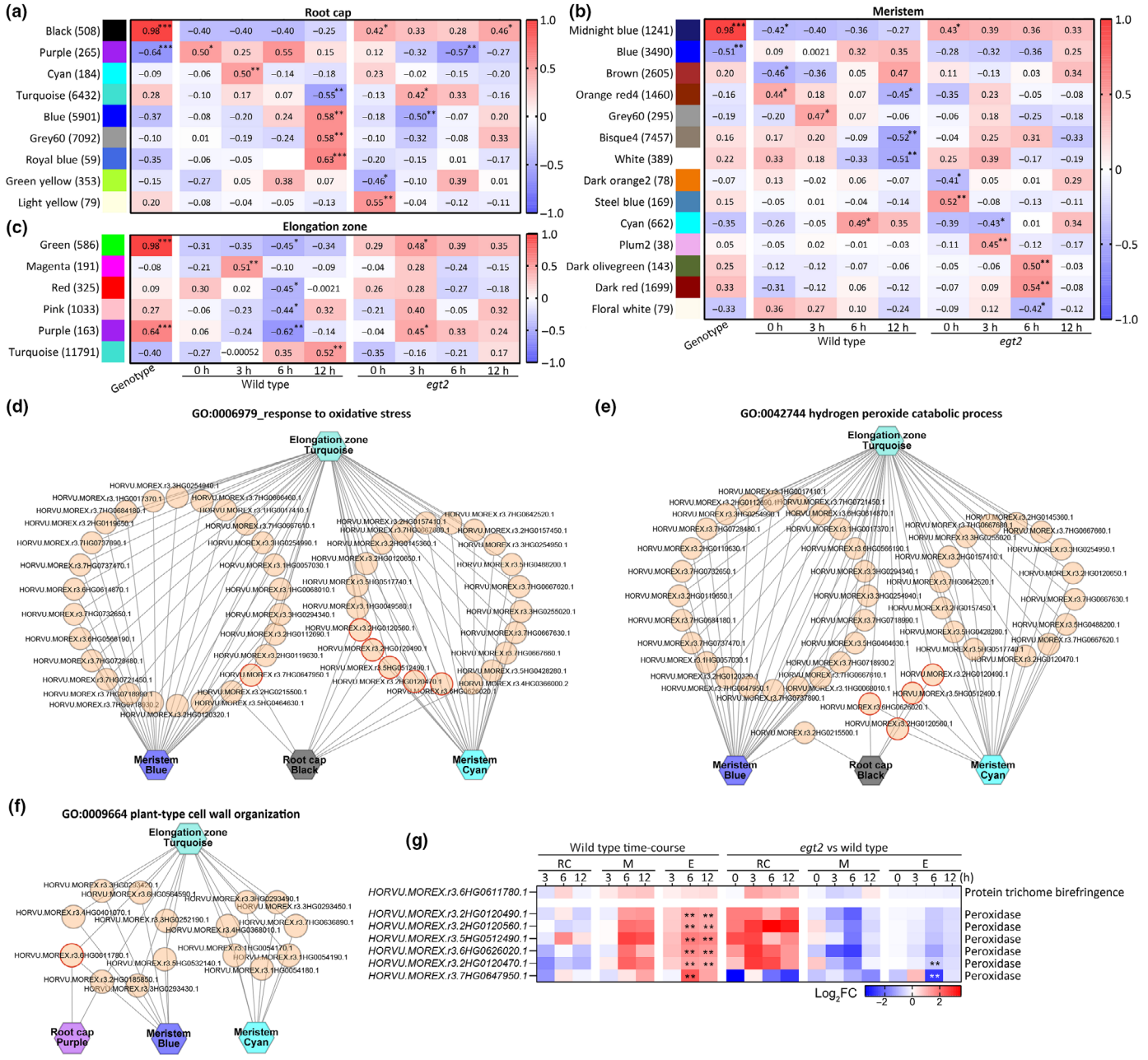

Fig. 5 Module-trait associations and genes assigned to plant cell wall and reactive oxygen species (ROS)-related processes in each selected module. (a–c) Module–trait relationships in the root cap (a), the meristem (b), and the elongation zone (c). The genotypes (WT and *egt2*) and time points (0, 3, 6 and 12 h) after gravistimulation are used as traits, each column corresponds to a different trait. Each row corresponds to the characteristic genes of the module. The relationship between the modules and traits is indicated in cell by Pearson's correlation coefficients. Asterisks indicate significant values calculated using the corPvalueStudent function: *, $P < 0.05$; **, $P < 0.01$; ***, $P < 0.001$. Cell color ranges from red (highly positive correlation) to blue (highly negative correlation). The number of genes contained in each module is indicated in brackets next to the module names. (d) Genes associated with 'response to oxidative stress'. (e) Genes associated with 'hydrogen peroxide catabolic process'. (f) Genes associated with 'plant-type cell wall organization'. (d–f) Hexagonal nodes represent modules, circle nodes in orange represent individual genes. Nodes encircled in dark orange represent genes determined in all three root zones. (g) The expression patterns of genes encircled in dark orange in (d–f) in the WT gravistimulation time-course experiments (WT time-course) and in the pairwise comparisons of *egt2* with WT (*egt2* vs WT). **, false discovery rate (FDR) < 5%.

epidermal cells infiltrated with constructs containing nYFP-OMT, nYFP-GXM, and nYFP-HMT together with the full-length coding sequence of EGT2 including a stop codon (+TGA) N-terminally fused to cYFP (Fig. S6: EGT2 (+TGA)-cYFP). The stop codon after EGT2 in this construct disables translation of cYFP. Remarkably, while OMT interaction with EGT2 was observed in the nucleus and in the cytoplasm (Fig. 6b) as expected from the subcellular localization experiments of these two proteins (Fig. 6a). By contrast, interaction of GXM and HMT with EGT2 occurred only in the nucleus (Fig. 6b), although these proteins are localized in the nucleus and cytoplasm (Fig. 6a).

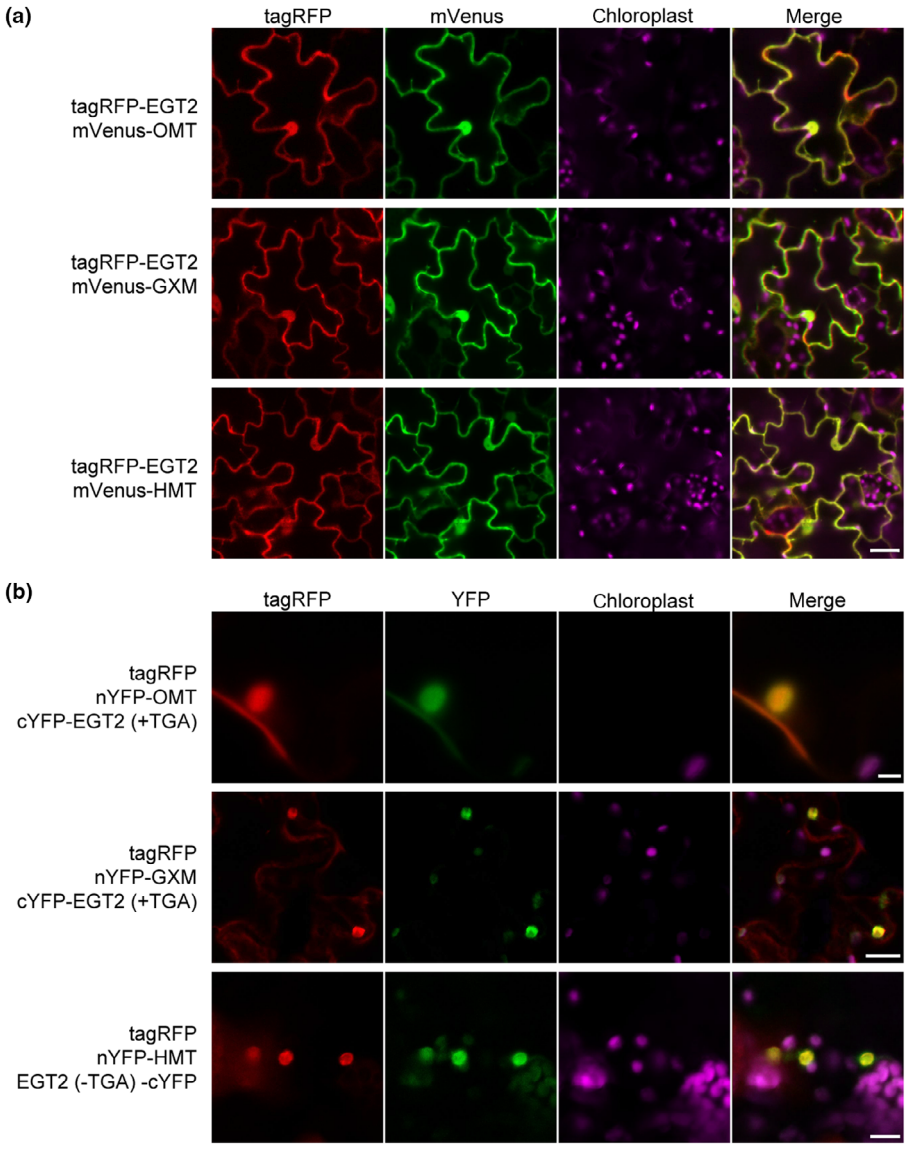

Fig. 6 Confirmation of interactions between EGT2 and other proteins. (a) Subcellular localization assay of EGT2 and interaction partners. tagRFP, red fluorescence; mVenus, yellow fluorescence. Bar, 50 μm. (b) Bimolecular fluorescence complementation assay of EGT2 and interaction partners. tagRFP, red fluorescence; mVenus, yellow fluorescence; nYFP, N-terminal part of YFP; cYFP, C-terminal part of YFP; EGT2 (+TGA), full-length coding sequence of EGT2; EGT2 (−TGA), coding sequence of EGT2 removed stop codon. Bars: (top) 10 μm; (middle) 50 μm; (bottom) 25 μm. (a, b) OMT, HORVU.MOREX.r3.3HG0330120.1; GXM, HORVU.MOREX.r3.7HG0749870.1; HMT, HORVU.MOREX.r3.2HG0126380.1; chloroplasts, autofluorescence of chloroplasts.

Discussion

Gravitropism modulates root system architecture by controlling the distribution of roots in different soil layers and thus their ability to absorb water and nutrients. Understanding the molecular mechanisms underlying root gravitropism will help to develop root ideotypes that can improve crop performance under unfavorable environmental conditions.

The root gravitropic response includes the perception of gravity signals mainly in the root cap, signal transduction through the meristem, and signal execution translating into a bending response in the elongation zone (Singh *et al.*, 2017; Su *et al.*, 2017; Nakamura *et al.*, 2019). We observed that the angle adjustment of WT barley roots was adjusted by 10° after 3 h of rotation and reached 30° (> 60% of the total adjusted angle) after 12 h of rotation (Fig. 1b; Kirschner *et al.*, 2021). In this study, we performed RNA-seq of the root cap, the meristem, and the elongation zone of WT barley roots before gravistimulation and 3, 6, and 12 h after reorientation of the roots by 90°. This experiment revealed transcriptomic variation in every step of gravitropic response at different time points. First, only a few DEGs were observed after 3 h of rotation in all three zones (Fig. 2a). This indicates that gravistimulation caused only little transcriptome adjustment at early stages of the experiment (Fig. 2b,c). Second, the elongation zone displayed by far the most DEGs (Fig. 2a,c), suggesting that gravitropic bending is subject to a more extensive transcriptomic regulation in the elongation zone than gravity perception in the root cap and signal transduction in the meristem.

Gene Ontology term analyses revealed the enrichment of a number of biological processes among the DEGs in the gravistimulated root cap and elongation zone. Gene Ontology terms related to ROS biosynthesis, cytoplasmic microtubule organization, plant transmembrane transport, carbohydrate metabolic, and calcium-mediated signaling were overrepresented in downregulated genes in root cap (Table S5a). These enriched GO

terms are in line with the notion that ROS (Krieger *et al.*, 2016), starch-related processes (Li *et al.*, 2020), dynamic actin-filament network (Hou *et al.*, 2003), and calcium (Bizet *et al.*, 2018) are involved in gravity sensing, which occurs primarily in root cap (Su *et al.*, 2020). In addition, the homolog of *AtLZY2* and *AtLZY3* and the homolog of *ZmCIPK15* were significantly downregulated in the root cap after 12 h of gravistimulation (Table S2). This is consistent with the role of *AtLZY2* and *AtLZY3* in root columella cells during gravitropic response and the function of *ZmCIPK15* in regulating maize root angles (Taniguchi *et al.*, 2017; Schneider *et al.*, 2022). In the elongation zone, seven cell wall, ROS, and protein phosphorylation-related terms were assigned to more than three gene clusters with DEG patterns (Table S5b). This is consistent with the observation that gravity changes lead to alterations in the shape of endodermal cells and in the transcript levels of genes associated with cell wall modifications (Johnson *et al.*, 2015, 2017). Moreover, cell wall-related processes are closely related to asymmetric cell elongation in the distal elongation zone of gravistimulated roots (Su *et al.*, 2017; Lešková *et al.*, 2020). It has also been demonstrated that gravistimulation induces an asymmetric distribution of ROS in the distal elongation zone of the root (higher in the lower flanks), which promotes root gravitropic bending (Krieger *et al.*, 2016). Furthermore, ROS production is also involved in regulating cell wall loosening and cell expansion (Liszkay *et al.*, 2004; Xiong *et al.*, 2015; Mabuchi *et al.*, 2018). Protein phosphorylation functions in mediating auxin biosynthesis, transport, and signaling, therefore playing a critical role in many auxin-related processes, including root gravitropism (Tan *et al.*, 2021).

In a previous study, we identified the barley mutant *egt2*, which shows enhanced root gravitropism (Kirschner *et al.*, 2021). RNA-seq of vertically grown roots showed that cell wall-related processes were affected in the mutant; however, nothing is known about the dynamics of the gravity response in regard to the role of EGT2 (Kirschner *et al.*, 2021). Here, we determined DEGs between different root zones of the gravistimulated roots of *egt2* and WT in a time-course experiment (Fig. 3). In the root cap, only 3% of gravity-responsive genes were regulated by *EGT2* (Fig. 4a), implying that *EGT2* might not play an important role in gravity perception in the root cap. This is in line with our previous observation that there was no significant difference in amyloplast content and their sedimentation rates between WT and *egt2* (Kirschner *et al.*, 2021). Similarly, there was no overlap between gravity-responsive genes and genes regulated by *EGT2* in the meristem suggesting that the role of *EGT2* in gravity signal transduction is not prominent on the transcriptomic level. In our previous study, we suggested that *EGT2* mediates gravity signal transduction at the protein level, further regulating the targets in the elongation zone to control the root gravitropism (Kirschner *et al.*, 2021). Consistently, in the elongation zone of *egt2*, gravistimulation induced the differential expression of thousands of *EGT2*-regulated genes (Fig. 3a,d). Intriguingly, > 1000 *EGT2*-regulated genes in the elongation zone were also regulated by gravistimulation in the WT roots (Fig. 4b). This implies that around one-third of gravity-responsive genes in the elongation zone of WT roots were regulated by *EGT2*, suggesting a critical role of *EGT2* in regulating root gravitropic bending. Plant cell wall organization and ROS-related GO terms that were assigned to these intersected genes in the elongation zone (Fig. S4b) support this hypothesis.

The *egt2* mutation results in an enhanced gravitropic response in barley roots, suggesting that *EGT2* might play a positive role in regulating antigravitropic offset (AGO), which counteracts gravitropism to regulate the root growth direction (Fig. 1b; Kawamoto *et al.*, 2020; Kirschner *et al.*, 2021; Fusi *et al.*, 2022). Based on this hypothesis, *EGT2* might suppress the expression of gravity-responsive genes that play a positive role in root gravitropism and induce the expression of gravity-responsive genes that negatively regulate root gravitropism. According to this hypothesis, mutation of *EGT2* would result in an opposite expression pattern of AGO-related genes in the *egt2* mutant than in the WT. Consistently, almost all of *EGT2*-regulated gravity-responsive genes were regulated in the opposite direction in the WT gravistimulation time-course experiment and in pairwise comparisons of *egt2* and WT roots (Table S7). This result supports the notion that *EGT2* mediates root gravitropism through the regulation of AGO and provides a number of candidate genes that might be involved in *EGT2*-depedent regulation of AGO, thus contributing to the understanding of the largely unknown mechanism of AGO.

Co-expression network analyses revealed that specific modules that have a strong correlation with genotype in all three root zones. These modules were in most cases contrastingly correlated with the gravitropic response of WT and *egt2* (Figs 5a–c, S5a–c). Genes in these modules are potential components involved in regulating gravitropic response and AGO (Fig. S5e–g; Kawamoto *et al.*, 2020; Fusi *et al.*, 2022). Moreover, modules correlated only with WT or *egt2* at some time point after gravistimulation might be involved in *EGT2*-independent or *EGT2*-dependent gravitropism, respectively. This result complements differential expression analyses, in particular for the root cap and the meristem where fewer gravity or *EGT2*-regulated genes were discovered (Figs 2, 3). In the elongation zone, many hub genes of significantly correlated modules were regulated by gravity and/or *EGT2* (Fig. S5g), which is in line with the differential expression analyses. Plant cell wall and ROS-related GO terms were assigned to modules strongly correlated with genotype in all three root zones (Fig. S5d). This is consistent with GO analyses of gravity and *EGT2*-regulated genes in the elongation zone (Fig. S4b), suggesting that plant cell wall and ROS-related processes might be involved in *EGT2*-controlled root gravitropic response. Moreover, six genes encoding peroxidases were present in significantly correlated modules in all three root zones (Fig. 5g). These results suggest that gravitropism regulation of *EGT2* might be similar to that of *EGT1*, which was proposed to control cell wall stiffness by regulating peroxidase and cell wall loosening-related enzymes, therefore mediating AGO (Fusi *et al.*, 2022).

Localization of EGT2 in the cytoplasm and nucleus was consistent with the predicted localization of its homologs in Arabidopsis (Denay *et al.*, 2017). As the only annotated domain in EGT2, the SAM domain is known as a protein–protein interaction domain in animals (Kim & Bowie, 2003). Recent studies on plant SAM

domain-containing proteins have provided initial insights into the interaction capabilities of the plant SAM domain (Murcha *et al.*, 2016; Sayou *et al.*, 2016). In the current study, we identified 79 proteins as putative interaction partners of EGT2 (Fig. S2c). The number of observed interaction candidates that responded to gravistimulation on basis of the transcriptome analyses was significantly higher than expected by chance (Fig. S2e), highlighting the role of EGT2 in root gravitropic response.

Bimolecular fluorescence complementation confirmed the interaction between EGT2 and three interaction candidates encoded by DEGs (Fig. 6). Two candidates were not confirmed, probably due to changes in protein structure caused by inappropriate terminal fusion to fluorescent proteins. Alternatively, the two proteins might be false-positive results of the yeast-two-hybrid experiment (Xing *et al.*, 2016). EGT2 fused with cYFP at the N-terminus (cYFP-EGT2 (+TGA)) displayed interaction with OMT and GXM, whereas EGT2 fused with cYFP at the C-terminus (EGT2 (−TGA)-cYFP) displayed interaction with HMT (Fig. 6b). This suggests that the interaction site of EGT2 with OMT or GXM might be different from that of EGT2 with HMT. None of the three independently confirmed proteins has been yet functionally characterized in barley. OMT is annotated as an '*O*-methyltransferase', while GXM is annotated as 'Glucuronoxylan 4-*O*-methyltransferase' and HMT is annotated as a heavy metal transport/detoxification superfamily protein.

Remarkably, while OMT interaction with EGT2 was observed in the nucleus and in the cytoplasm as expected from their subcellular localization, interaction of GXM and HMT with EGT2 occurred only in the nucleus, although these proteins are also localized in the nucleus and cytoplasm. One explanation for the confined interaction of GXM and HMT with EGT2 in the nucleus could be that their interaction needs a hypothetical co-factor that is present only in the nucleus but not the cytoplasm. Hence, the detailed function of these proteins in the determination of the setpoint angle of barley seminal roots by interacting with EGT2 remains to be investigated in future studies.

Acknowledgements

We would like to thank Andreas Meyer (University of Bonn) and Peng Yu (University of Bonn) for their discussions and suggestions on this project. We would also like to thank Helmut Rehkopf (University of Bonn) and Christa Schulz (University of Bonn) for their experimental support of this study. This work was funded by the Deutsche Forschungsgemeinschaft (DFG) grant HO2249/21-1 to FH. Open Access funding enabled and organized by Projekt DEAL.

Competing interests

None declared.

Author contributions

LG and FH conceived the experiments. LG performed the experiments, analyzed and interpreted the data and drafted the article. AK was involved in the bioinformatic analyses of RNA-seq data. MB was involved in the yeast-two-hybrid experiments. GKK and SS participated in data interpretation and revised the article. FH coordinated the study, participated in data interpretation and drafting of the article. All authors approved the final draft.

ORCID

Marcel Baer https://orcid.org/0000-0001-7708-7202
Li Guo https://orcid.org/0000-0003-0406-6966
Frank Hochholdinger https://orcid.org/0000-0002-5155-0884
Alina Klaus https://orcid.org/0000-0003-0805-2860
Silvio Salvi https://orcid.org/0000-0002-0338-8894

Data availability

RNA-seq data have been deposited in the SRA under accession no. PRJNA858009 (https://www.ncbi.nlm.nih.gov/bioproject/858009).

References

Alexa A, Rahnenführer J. 2022. *TOPGO: enrichment analysis for gene ontology*. R package v.2.50.0. [WWW document] URL https://bioconductor.org/packages/release/bioc/html/topGO.html [accessed 13 January 2023].

Baluška F, Mancuso S, Volkmann D, Barlow PW. 2010. Root apex transition zone: a signalling–response nexus in the root. *Trends in Plant Science* **15**: 402–408.

Benjamini Y, Hochberg Y. 1995. Controlling the false discovery rate: a practical and powerful approach to multiple testing. *Journal of the Royal Statistical Society: Series B (Methodological)* **57**: 289–300.

Bizet F, Pereda-Loth V, Chauvet H, Gérard J, Eche B, Girousse C, Courtade M, Perbal G, Legué V. 2018. Both gravistimulation onset and removal trigger an increase of cytoplasmic free calcium in statocytes of roots grown in microgravity. *Scientific Reports* **8**: 1–10.

Chen H, Boutros PC. 2011. VENNDIAGRAM: a package for the generation of highly-customizable Venn and Euler diagrams in R. *BMC Bioinformatics* **12**: 35.

Conway JR, Lex A, Gehlenborg N. 2017. UPSETR: an R package for the visualization of intersecting sets and their properties. *Bioinformatics* **33**: 2938–2940.

Denay G, Vachon G, Dumas R, Zubieta C, Parcy F. 2017. Plant SAM-domain proteins start to reveal their roles. *Trends in Plant Science* **22**: 718–725.

Eriksson S, Böhlenius H, Moritz T, Nilsson O. 2006. GA_4 is the active gibberellin in the regulation of *LEAFY* transcription and *Arabidopsis* floral initiation. *Plant Cell* **18**: 2172–2181.

Fusi R, Rosignoli S, Lou H, Sangiorgi G, Bovina R, Pattem JK, Borkar AN, Lombardi M, Forestan C, Milner SG *et al.* 2022. Root angle is controlled by *EGT1* in cereal crops employing an antigravitropic mechanism. *Proceedings of the National Academy of Sciences, USA* **119**: e2201350119.

Gietz RD, Schiestl RH, Willems AR, Woods RA. 1995. Studies on the transformation of intact yeast cells by the LiAc/SS-DNA/PEG procedure. *Yeast* **11**: 355–360.

Grefen C, Blatt MR. 2012. A 2in1 cloning system enables ratiometric bimolecular fluorescence complementation (rBiFC). *BioTechniques* **53**: 311–314.

Hollender CA, Pascal T, Tabb A, Hadiarto T, Srinivasan C, Wang W, Liu Z, Scorza R, Dardick C. 2018. Loss of a highly conserved sterile alpha motif domain gene (*WEEP*) results in pendulous branch growth in peach trees. *Proceedings of the National Academy of Sciences, USA* **115**: E4690–E4699.

Hou G, Mohamalawari DR, Blancaflor EB. 2003. Enhanced gravitropism of roots with a disrupted cap actin cytoskeleton. *Plant Physiology* **131**: 1360–1373.

Jiao Z, Du H, Chen S, Huang W, Ge L. 2021. *LAZY* gene family in plant gravitropism. *Frontiers in Plant Science* **11**: 2096.

Johnson CM, Subramanian A, Edelmann RE, Kiss JZ. 2015. Morphometric analyses of petioles of seedlings grown in a spaceflight experiment. *Journal of Plant Research* **128**: 1007–1016.

Johnson CM, Subramanian A, Pattathil S, Correll MJ, Kiss JZ. 2017. Comparative transcriptomics indicate changes in cell wall organization and stress response in seedlings during spaceflight. *American Journal of Botany* **104**: 1219–1231.

Johnson JM, Kohler AR, Haus MJ, Hollender CA. 2022. Arabidopsis *weep* mutants exhibit narrow root angles. *microPublication Biology*. doi: 10.17912/micropub.biology.000584.

Jones AM, Xuan Y, Xu M, Wang RS, Ho CH, Lalonde S, You CH, Sardi MI, Parsa SA, Smith-Valle E *et al.* 2014. Border control – a membrane-linked interactome of Arabidopsis. *Science* **344**: 711–716.

Kawamoto N, Kanbe Y, Nakamura M, Mori A, Terao Morita M. 2020. Gravity-sensing tissues for gravitropism are required for "anti-gravitropic" phenotypes of *lzy* multiple mutants in Arabidopsis. *Plants* **9**: 615.

Kim CA, Bowie JU. 2003. SAM domains: uniform structure, diversity of function. *Trends in Biochemical Sciences* **28**: 625–628.

Kirschner GK, Rosignoli S, Guo L, Vardanega I, Imani J, Altmüller J, Milner SG, Balzano R, Nagel KA, Pflugfelder D *et al.* 2021. *ENHANCED GRAVITROPISM 2* encodes a STERILE ALPHA MOTIF-containing protein that controls root growth angle in barley and wheat. *Proceedings of the National Academy of Sciences, USA* **118**: e2101526118.

Krieger G, Shkolnik D, Miller G, Fromm H. 2016. Reactive oxygen species tune root tropic responses. *Plant Physiology* **172**: 1209–1220.

Langfelder P, Horvath S. 2008. WGCNA: an R package for weighted correlation network analysis. *BMC Bioinformatics* **9**: 559.

Lešková A, Zvarík M, Araya T, Giehl RFH. 2020. Nickel toxicity targets cell wall-related processes and PIN2-mediated auxin transport to inhibit root elongation and gravitropic responses in Arabidopsis. *Plant and Cell Physiology* **61**: 519–535.

Li Y, Yuan W, Li L, Miao R, Dai H, Zhang J, Xu W. 2020. Light-dark modulates root hydrotropism associated with gravitropism by involving amyloplast response in Arabidopsis. *Cell Reports* **32**: 108198.

Liszkay A, Van Der Zalm E, Schopfer P. 2004. Production of reactive oxygen intermediates ($O_2^{\bullet-}$, H_2O_2, and $^{\bullet}OH$) by maize roots and their role in wall loosening and elongation growth. *Plant Physiology* **136**: 3114–3123.

Mabuchi K, Maki H, Itaya T, Suzuki T, Nomoto M, Sakaoka S, Morikami A, Higashiyama T, Tada Y, Busch W *et al.* 2018. MYB30 links ROS signaling, root cell elongation, and plant immune responses. *Proceedings of the National Academy of Sciences, USA* **115**: E4710–E4719.

Maechler M, Rousseeuw P, Struyf A, Hubert M, Hornik K. 2022. *CLUSTER: cluster analysis basics and extensions*. R package v.2.1.3. [WWW document] URL https://cran.r-project.org/web/packages/cluster/index.html [accessed 13 January 2023].

Mancuso S, Barlow PW, Volkmann D, Baluska F. 2006. Actin turnover-mediated gravity response in maize root apices. *Plant Signaling & Behavior* **1**: 52–58.

Mascher M, Wicker T, Jenkins J, Plott C, Lux T, Koh CS, Ens J, Gundlach H, Boston LB, Tulpová Z *et al.* 2021. Long-read sequence assembly: a technical evaluation in barley. *Plant Cell* **33**: 1888–1906.

Murcha MW, Kubiszewski-Jakubiak S, Teixeira PF, Gügel IL, Kmiec B, Narsai R, Ivanova A, Megel C, Schock A, Kraus S *et al.* 2016. Plant-specific preprotein and amino acid transporter proteins are required for tRNA import into mitochondria. *Plant Physiology* **172**: 2471–2490.

Nakamura M, Nishimura T, Morita MT. 2019. Gravity sensing and signal conversion in plant gravitropism. *Journal of Experimental Botany* **70**: 3495–3506.

Osthoff A, Donà dalle Rose P, Baldauf JA, Piepho H-P, Hochholdinger F. 2019. Transcriptomic reprogramming of barley seminal roots by combined water deficit and salt stress. *BMC Genomics* **20**: 1–14.

Qiao F, Bowie JU. 2005. The many faces of SAM. *Science's STKE* **2005**: re7.

Ray S, Chee L, Matson DR, Palermo NY, Bresnick EH, Hewitt KJ. 2020. Sterile alpha motif domain requirement for cellular signaling and survival. *Journal of Biological Chemistry* **295**: 7113–7125.

Ritchie ME, Phipson B, Wu D, Hu Y, Law CW, Shi W, Smyth GK. 2015. LIMMA powers differential expression analyses for RNA-sequencing and microarray studies. *Nucleic Acids Research* **43**: E47.

Robinson MD, McCarthy DJ, Smyth GK. 2010. EDGER: a BIOCONDUCTOR package for differential expression analysis of digital gene expression data. *Bioinformatics* **26**: 139–140.

Ronzier E, Corratgé-Faillie C, Sanchez F, Prado K, Brière C, Leonhardt N, Thibaud JB, Xiong TC. 2014. CPK13, a noncanonical Ca^{2+}-dependent protein kinase, specifically inhibits KAT2 and KAT1 shaker K^+ channels and reduces stomatal opening. *Plant Physiology* **166**: 314–326.

Sayou C, Nanao MH, Jamin M, Posé D, Thévenon E, Grégoire L, Tichtinsky G, Denay G, Ott F, Peirats Llobet M *et al.* 2016. A SAM oligomerization domain shapes the genomic binding landscape of the LEAFY transcription factor. *Nature Communications* **7**: 11222.

Schneider HM, Lor VSN, Hanlon MT, Perkins A, Kaeppler SM, Borkar AN, Bhosale R, Zhang X, Rodriguez J, Bucksch A *et al.* 2022. Root angle in maize influences nitrogen capture and is regulated by calcineurin B-like protein (CBL)-interacting serine/threonine-protein kinase 15 (ZmCIPK15). *Plant, Cell & Environment* **45**: 837–853.

Schultz J, Ponting CP, Hofmann K, Bork P. 1997. SAM as a protein interaction domain involved in developmental regulation. *Protein Science* **6**: 249–253.

Singh M, Gupta A, Laxmi A. 2017. Striking the right chord: signaling enigma during root gravitropism. *Frontiers in Plant Science* **8**: 1304.

Siriwardana NS, Lamb RS. 2012. The poetry of reproduction: the role of LEAFY in *Arabidopsis thaliana* flower formation. *International Journal of Developmental Biology* **56**: 207–221.

Su SH, Gibbs NM, Jancewicz AL, Masson PH. 2017. Molecular mechanisms of root gravitropism. *Current Biology* **27**: R964–R972.

Su SH, Keith MA, Masson PH. 2020. Gravity signaling in flowering plant roots. *Plants* **9**: 1–23.

Supek F, Bošnjak M, Škunca N, Šmuc T. 2011. REVIGO summarizes and visualizes long lists of gene ontology terms. *PLoS ONE* **6**: e21800.

Tan S, Luschnig C, Friml J. 2021. Pho-view of auxin: reversible protein phosphorylation in auxin biosynthesis, transport and signaling. *Molecular Plant* **14**: 151–165.

Taniguchi M, Furutani M, Nishimura T, Nakamura M, Fushita T, Iijima K, Baba K, Tanaka H, Toyota M, Tasaka M *et al.* 2017. The Arabidopsis LAZY1 family plays a key role in gravity signaling within statocytes and in branch angle control of roots and shoots. *Plant Cell* **29**: 1984–1999.

Verbelen JP, De Cnodder T, Le J, Vissenberg K, Baluška F. 2006. The root apex of *Arabidopsis thaliana* consists of four distinct zones of growth activities. *Plant Signaling & Behavior* **1**: 296–304.

Wolverton C, Mullen JL, Ishikawa H, Evans ML. 2002. Root gravitropism in response to a signal originating outside of the cap. *Planta* **215**: 153–157.

Xing S, Wallmeroth N, Berendzen KW, Grefen C. 2016. Techniques for the analysis of protein–protein interactions *in vivo*. *Plant Physiology* **171**: 727–758.

Xiong J, Yang Y, Fu G, Tao L. 2015. Novel roles of hydrogen peroxide (H_2O_2) in regulating pectin synthesis and demethylesterification in the cell wall of rice (*Oryza sativa*) root tips. *New Phytologist* **206**: 118–126.

Yamaguchi N. 2021. LEAFY, a pioneer transcription factor in plants: a mini-review. *Frontiers in Plant Science* **12**: 1274.

Zhang Y, Xiao G, Wang X, Zhang X, Friml J. 2019. Evolution of fast root gravitropism in seed plants. *Nature Communications* **10**: 3480.

Supporting Information

Additional Supporting Information may be found online in the Supporting Information section at the end of the article.

Fig. S1 Quantification of meristem length of wild-type and *egt2* before and after 6 or 10 h of gravistimulation.

Fig. S2 Overview of yeast-two-hybrid screening.

Fig. S3 Dynamics of the expression profiles of graviregulated genes.

Fig. S4 Enriched GO terms for gravity-regulated genes that are *EGT2* related.

Fig. S5 Co-expression analysis.

Fig. S6 Control experiments for bimolecular fluorescence complementation analyses of EGT2 and interaction candidates.

Table S1 List of oligonucleotide primers.

Table S2 Overview of differentially expressed genes (FDR < 5%) in gravistimulated wild-type roots in a time-course experiment.

Table S3 Hierarchical clustering analysis of differentially expressed genes (FDR < 5%) in the root cap of gravistimulated wild-type roots.

Table S4 Hierarchical clustering analysis of differentially expressed genes (FDR < 5%) in elongation zone of gravistimulated wild-type roots.

Table S5 Enriched biological process terms among differentially expressed genes (FDR < 5%) in the root cap and elongation zone of gravistimulated wild-type roots.

Table S6 Overview of genes differentially expressed between wild-type and *egt2* (FDR < 5%) in a gravistimulation time-course experiment.

Table S7 Enriched biological processes terms among genes differentially expressed between wild-type and *egt2* (FDR < 5%) root caps, meristems, and elongation zones after a gravistimulation time-course experiment.

Table S8 Overlapping genes among differentially expressed genes in the wild-type (WT) time-course experiment and *egt2* vs WT comparisons.

Table S9 Overview of the candidates interacting with EGT2 as identified by yeast-two-hybrid screening.

Please note: Wiley is not responsible for the content or functionality of any Supporting Information supplied by the authors. Any queries (other than missing material) should be directed to the *New Phytologist* Central Office.